SUPPORTING INFORMATION

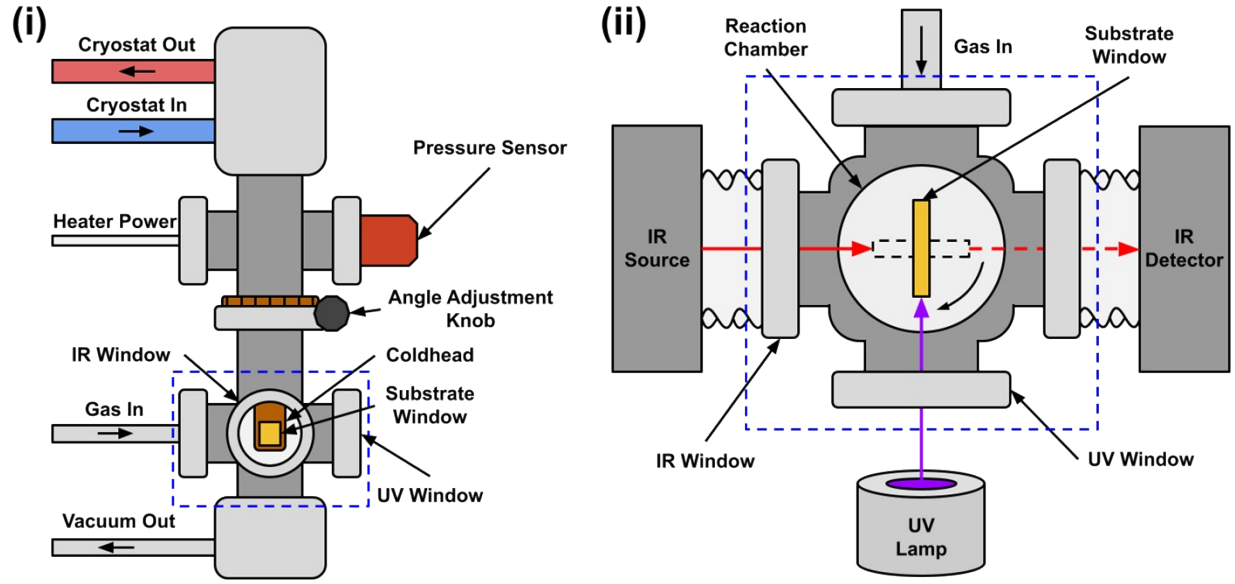

Figure S1a. A schematic diagram of (i) side view of the high-vacuum chamber used in this research project to generate molecular ice films from species deposited from the gas phase onto a KBr substrate and (ii) top-down view of the high-vacuum chamber, showing the two possible orientations of the substrate window (yellow rectangle and dashed line). The optical path of the IR beam through the chamber and external KBr windows is shown (red), as well as the entry of UV light from an external lamp through the MgF_2 window (purple).

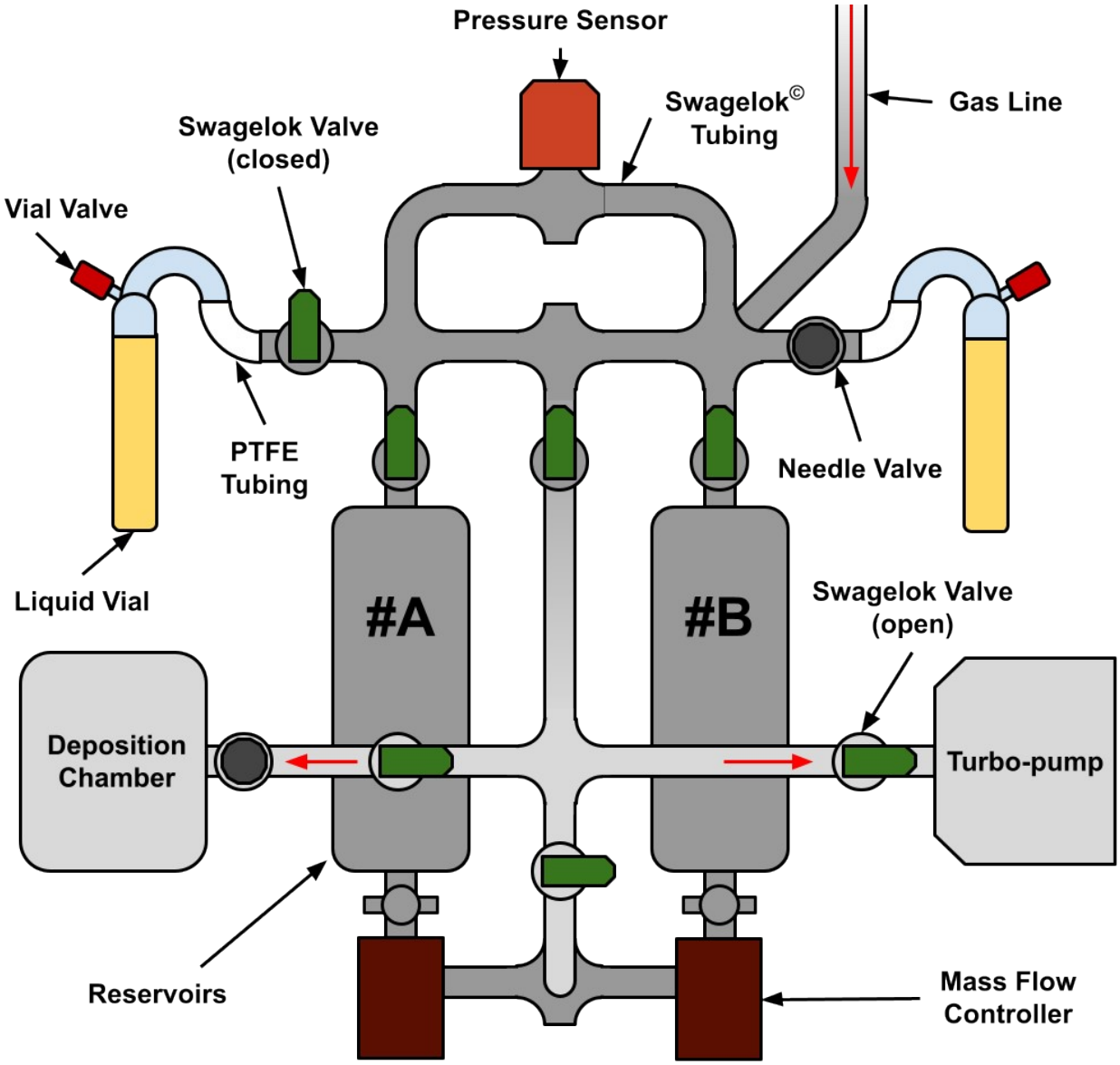

Figure S1b. A schematic representation of the gas manifold apparatus that stores and distributes sample gas provided from adjoining cylinders and/or liquid vials into the reaction chamber. Reservoir cylinders #A and #B allow separate retention and subsequent mixing of multiple gases.

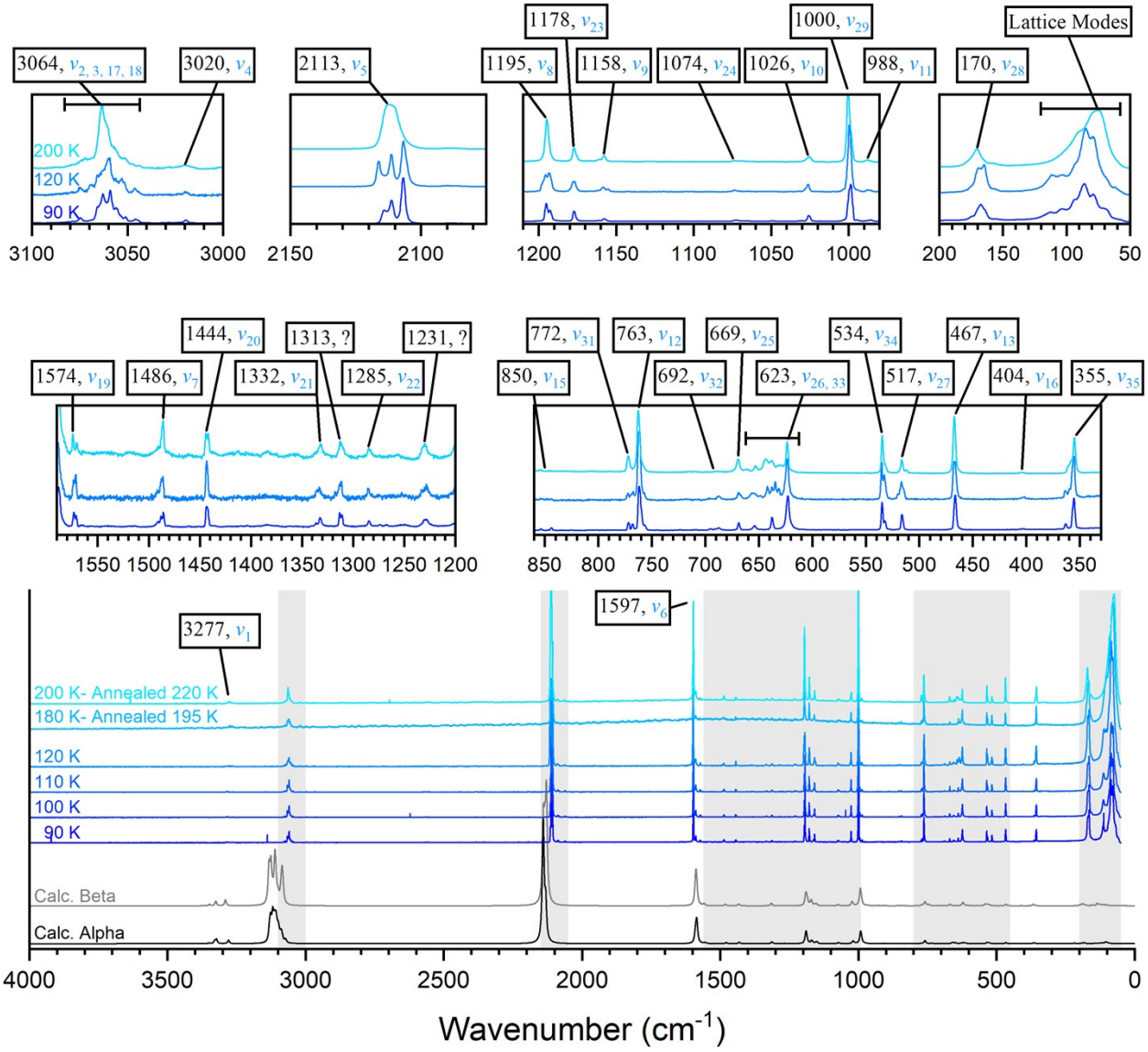

Figure S2. Raman spectra of pure phenylacetylene collected at between 90-120 K, and at 180 and 200 K after annealing at 195 and 220 K, respectively.

Table S1. Raman peak assignments for $C_6H_5C_2H$ ice at 90, 120, and 200 K. The 200 K spectrum was collected after annealing at 220 K for 3 minutes.

Peak (90 K) / cm^{-1}	**Peak (120 K) / cm^{-1}**	**Peak (200 K) / cm^{-1}**	**Assignment**	**Ref. †**
		3339	CB	
		3323, 3317	CB	
3283	3280	3294	ν_1	a
3274	3273	3277		
3263	3268, 3264	3268		
3074	3075, 3069	3072	ν_2, ν_3, ν_{17}, ν_{18}	a
3066, 3063	3066, 3063			
3059, 3056	3060, 3056	3064, 3058		
3051	3053	3052		
3046	3046	3048, 3044		
-	-	3029	CB	
3020	3020	3020	ν_4	a
2114, 2112	2116, 2111	2112	ν_5	a
2107	2107			
1952	1955	1952	CB	
1641	-	-	CB	
1628	-	-	CB	
1608			ν_6	a
1598	1598	1597		
1588	1589	1589		
1573, 1571	1573, 1571	1574, 1571	ν_{19}	a
1491	1491		ν_7	a
1488, 1486	1486	1486		
1443	1443	1444, 1442	ν_{20}	a
1337, 1333	1336, 1333	1332	ν_{21}	a
	1318		CB	
1313, 1311	1312	1313		
1285	1286	1285	ν_{22}	a
1229	1229	1231	CB	
1193, 1195	1196, 1193	1195	ν_8	a
1177	1178	1177	ν_{23}	a
1162, 1158	1162, 1158	1162, 1158	ν_9	a
	1155			
1073	1074	1073	ν_{24}	a
1026	1026	1025	ν_{10}	a
999, 994	1000	1000	ν_{29}	a
985	988	988	ν_{11}	a
854	854, 849	854	ν_{15}	a
844	844	844		
772, 768	772, 767	772	ν_{31}	a
762, 757	762	763	ν_{12}	a

695, 691 688	687	689	ν_{32}	a
669	669	669	ν_{25}	a
		661	ν_{26}, ν_{33}	a
654	656	653		
638	642, 638	644, 638		
	635, 631	629		
623	623	623		
535, 532	535, 533	534	ν_{34}	a
516	517	517, 512	ν_{27}	
466	467	467	ν_{13}	
403	402	405	ν_{16}	
363	363	361, 358	ν_{35}	
356	355	355		
174, 168	169, 165	170	ν_{28}	
156	157	157		
112, 104	112, 103		Lattice Modes	
94, 86	85	88		
79, 70, 57	79, 62	75		

Notes: † Peak assignments are compiled from liquid, amorphous and crystalline ice data published in (a, Chernia, 2000).

Table S2. $C_6H_5C_2H$ unit cell parameters and phase fraction for the Rietveld refinement of literature α-$C_6H_5C_2H$, β-$C_6H_5C_2H$, and γ-$C_6H_5C_2H$ unit cell against XRD diffraction patterns collected at 94 and 190 K (XRD experiment 1).

Lattice parameters	**α-$C_6H_5C_2H$**	**β-$C_6H_5C_2H$**	**γ-$C_6H_5C_2H$**
94 K pattern: Rw = 3.118%, GOF = 3.81			
a	5.77182 Å	5.85543 Å	40.84477 Å
b	8.76976 Å	9.3016 Å	5.85226 Å
c	15.97437 Å	18.3395 Å	32.35205 Å
α	74.322°	71.108°	90°
β	72.856°	82.98°	107.639°
γ	78.63°	78.951°	90°
Volume	737.819 $Å^3$	925.584 $Å^3$	7369.665 $Å^3$
Molar fraction	0.2363	10.59	1
Weight fraction	0.012	0.563	0.425
190 K pattern: Rw = 2.768%, GOF = 2.78			
a	5.71034 Å	6.1258 Å	41.13733 Å
b	9.12328 Å	9.21115 Å	5.78573 Å
c	15.50777 Å	18.27201 Å	32.6745 Å
α	77.132°	71.841°	90°
β	80.859°	86.122°	107.838°
γ	79.828°	83.24°	90°
Volume	769.199 $Å^3$	972.327 $Å^3$	7402.972 $Å^3$
Molar fraction	424.4	4.769	1
Weight fraction	0.965	0.013	0.022

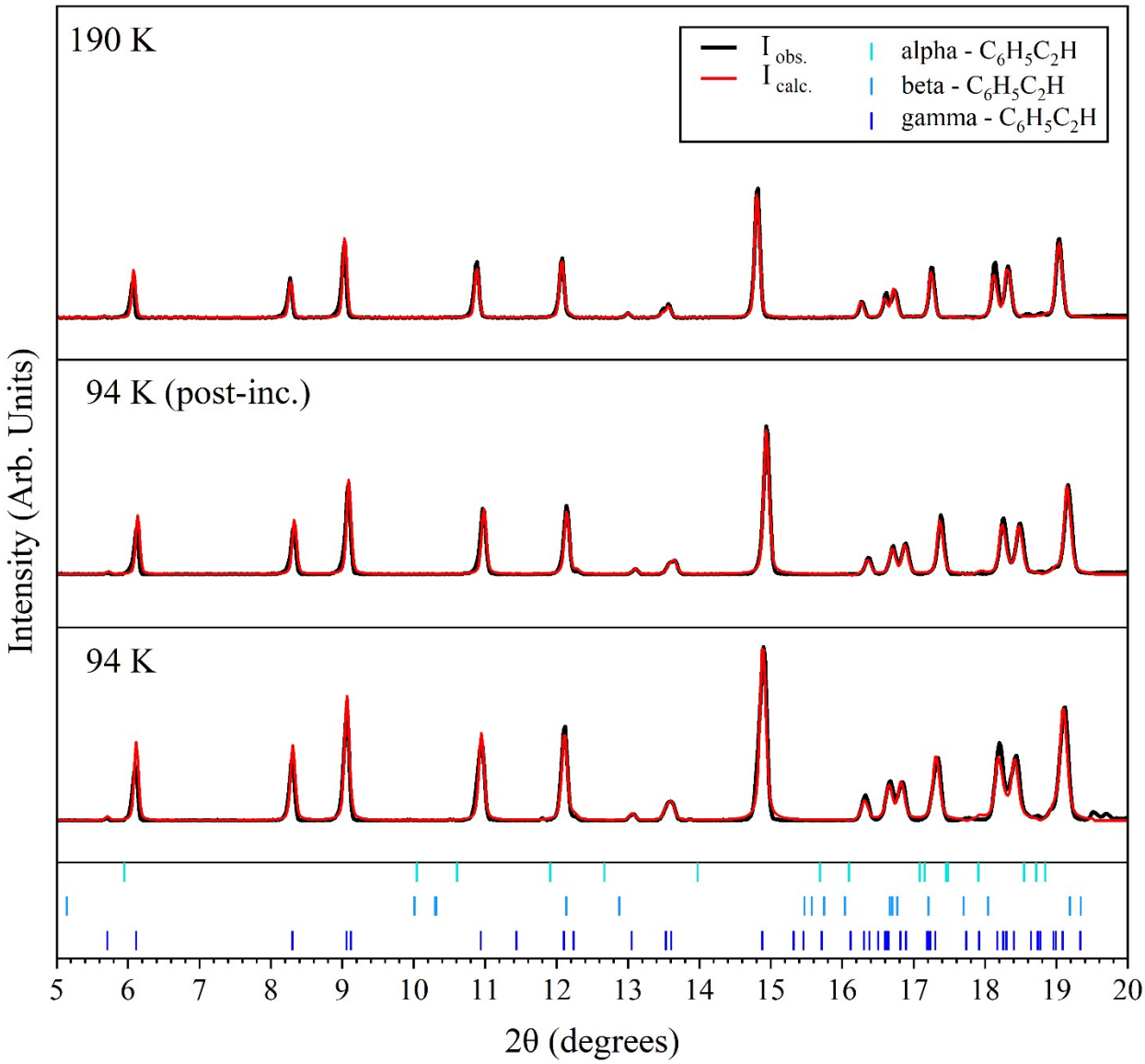

Figure S3. XRD patterns for phenylacetylene ice collected at 94 K before and after 2-hour incubation at 94, and collected at 190 K (bottom, middle, and top, respectively. λ = 1.54 Å). Plotted are the Rietveld refinement models (red; Rw = 24.841%, GOF = 8.09, Rw = 24.412%, GOF = 7.60, Rw = 24.313%, GOF = 7.61) and residual patterns (grey). Tick marks represent Bragg peak positions of α-phenylacetylene (teal), β-phenylacetylene (blue), and γ-phenylacetylene (dark blue).

Table S3. $C_6H_5C_2H$ unit cell parameters and phase fraction for the Rietveld refinement of the literature γ-$C_6H_5C_2H$ unit cell against XRD diffraction patterns collected at 94 K, at 94 K after incubation at constant temperature for two hours, and at 190 K (XRD experiment 2).

Lattice parameters	**α-$C_6H_5C_2H$**	**β-$C_6H_5C_2H$**	**γ-$C_6H_5C_2H$**
94 K pattern (pre-incubation): Rw = 24.841%, GOF = 8.09			
a	-	-	40.96643 Å
b	-	-	5.84339 Å
c	-	-	32.47098 Å
α	-	-	90°
β	-	-	107.738°
γ	-	-	90°
Volume	-	-	7403.465 Å^3
Molar fraction	0	0	1
94 K pattern (post-incubation): Rw = 24.313%, GOF = 7.61			
a	-	-	40.83996 Å
b	-	-	5.84077 Å
c	-	-	32.37016 Å
α	-	-	90°
β	-	-	107.704°
γ	-	-	90°
Volume	-	-	7355.792 Å^3
Molar fraction	0	0	1
190 K pattern: Rw = 24.412%, GOF = 7.60			
a	-	-	41.1273 Å
b	-	-	5.79273 Å
c	-	-	32.6583 Å
α	-	-	90°
β	-	-	107.861°
γ	-	-	90°
Volume	-	-	7405.478 Å^3
Molar fraction	0	0	1

Table S4. $C_6H_5C_2H$ unit cell parameters and phase fraction for the Rietveld refinement of literature α-$C_6H_5C_2H$ and γ-$C_6H_5C_2H$ unit cells against XRD diffraction patterns collected at 160 and 220 K.

Lattice parameters	**α-$C_6H_5C_2H$**	**β-$C_6H_5C_2H$**	**γ-$C_6H_5C_2H$**
160 K pattern: Rw = 3.118%, GOF = 3.81			
a	5.46178 Å	-	41.07975 Å
b	9.50312 Å	-	5.81989 Å
c	15.57896 Å	-	32.56623 Å
α	75.823°	-	90°
β	76.608°	-	107.862°
γ	72.754°	-	90°
Volume	737.613 $Å^3$	-	7410.638 $Å^3$
Molar fraction	0.57	0	1
Weight fraction	0.056	0	0.944
220 K pattern: Rw = 2.768%, GOF = 2.78			
a	5.84222 Å	-	40.823 Å
b	9.18218 Å	-	5.8721 Å
c	15.47201 Å	-	32.332 Å
α	77.486°	-	90°
β	81.317°	-	107.608°
γ	80.508°	-	90°
Volume	793.430 $Å^3$	-	7387.398 $Å^3$
Molar fraction	1	0	0.01
Weight fraction	0.912	0	0.088

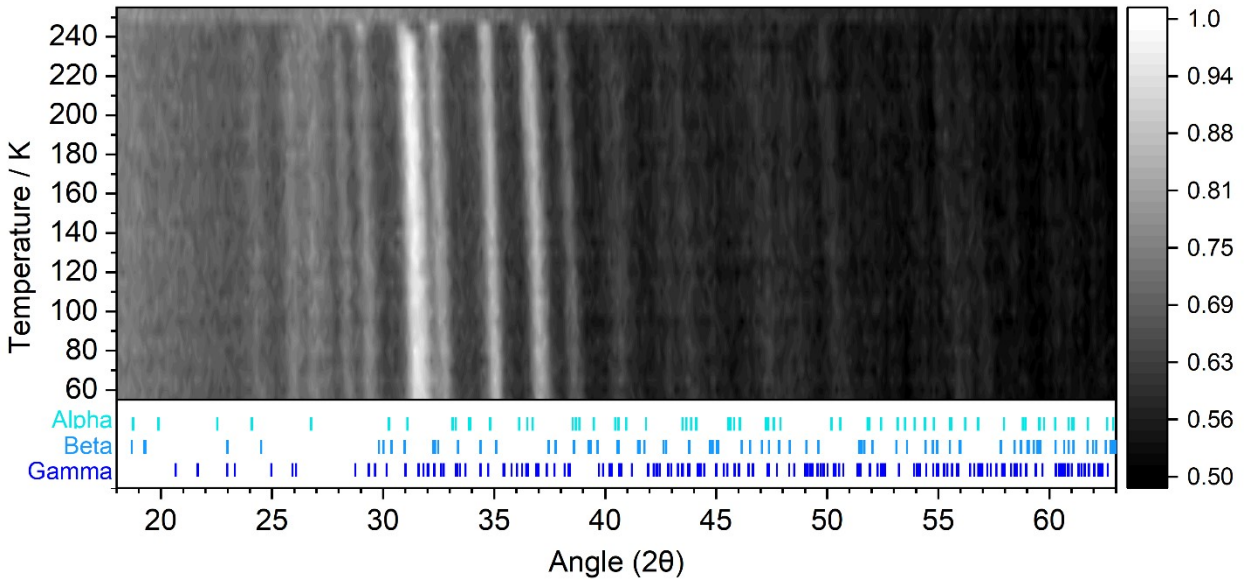

Figure S4. Thermodiffractogram of the neutron diffraction patterns of phenylacetylene ice collected in 5 K increments from 50-255 K for 2 min (λ = 2.413), where lightness represents peak intensity. Tick marks represent Bragg peak positions of α-phenylacetylene (teal), β-phenylacetylene (blue), and γ-phenylacetylene (dark blue).

Table S5. $C_6H_5C_2H$ unit cell parameters and phase fraction for the Rietveld refinement of literature α-$C_6H_5C_2H$ and β-$C_6H_5C_2H$ unit cells against neutron diffraction patterns collected at 50 and 160 K.

Lattice parameters	**α-$C_6H_5C_2H$**	**β-$C_6H_5C_2H$**	**γ-$C_6H_5C_2H$**
50 K pattern: Rw = 1.88%, GOF = 2.55			
a	5.6489 Å	5.69802 Å	-
b	8.98845 Å	9.01959 Å	-
c	15.09882 Å	18.04228 Å	-
α	76.807°	71.585°	-
β	81.471°	82.342°	-
γ	80.125°	78.596°	-
Volume	730.569 $Å^3$	859.908 $Å^3$	-
Molar fraction	1	1.987	0
Weight fraction	0.333	0.667	0
160 K pattern: Rw = 2.03%, GOF = 2.90			
a	5.73969 Å	5.69583 Å	-
b	8.96493 Å	9.11793 Å	-
c	15.20058 Å	18.25131 Å	-
α	76.375°	71.733°	-
β	81.636°	82.105°	-
γ	79.875°	78.281°	-
Volume	743.871 $Å^3$	878.565 $Å^3$	-
Molar fraction	1	1.987	0
Weight fraction	0.333	0.667	0

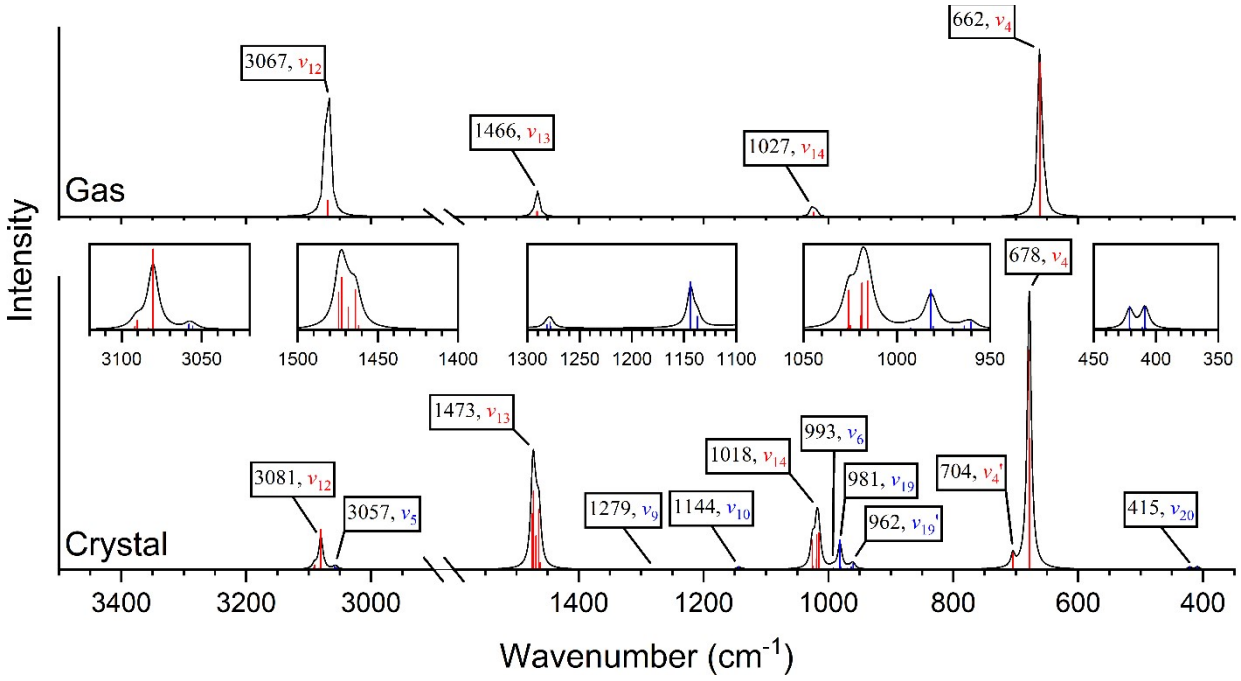

Figure S5. pDFT simulated IR spectra for gas-phase (top), and crystalline C_6H_6 (*Pbca*; bottom) at the B3LYP-D3 level of theory, with arbitrary absolute intensity. Peaks labelled according to H-M notation. The frequency of individual transitions formally IR-active in the gas-phase are shown in red, and transitions only formally IR-active in the crystal phase are shown in blue. Spectra incorporate an anharmonic scaling factor of 0.965.

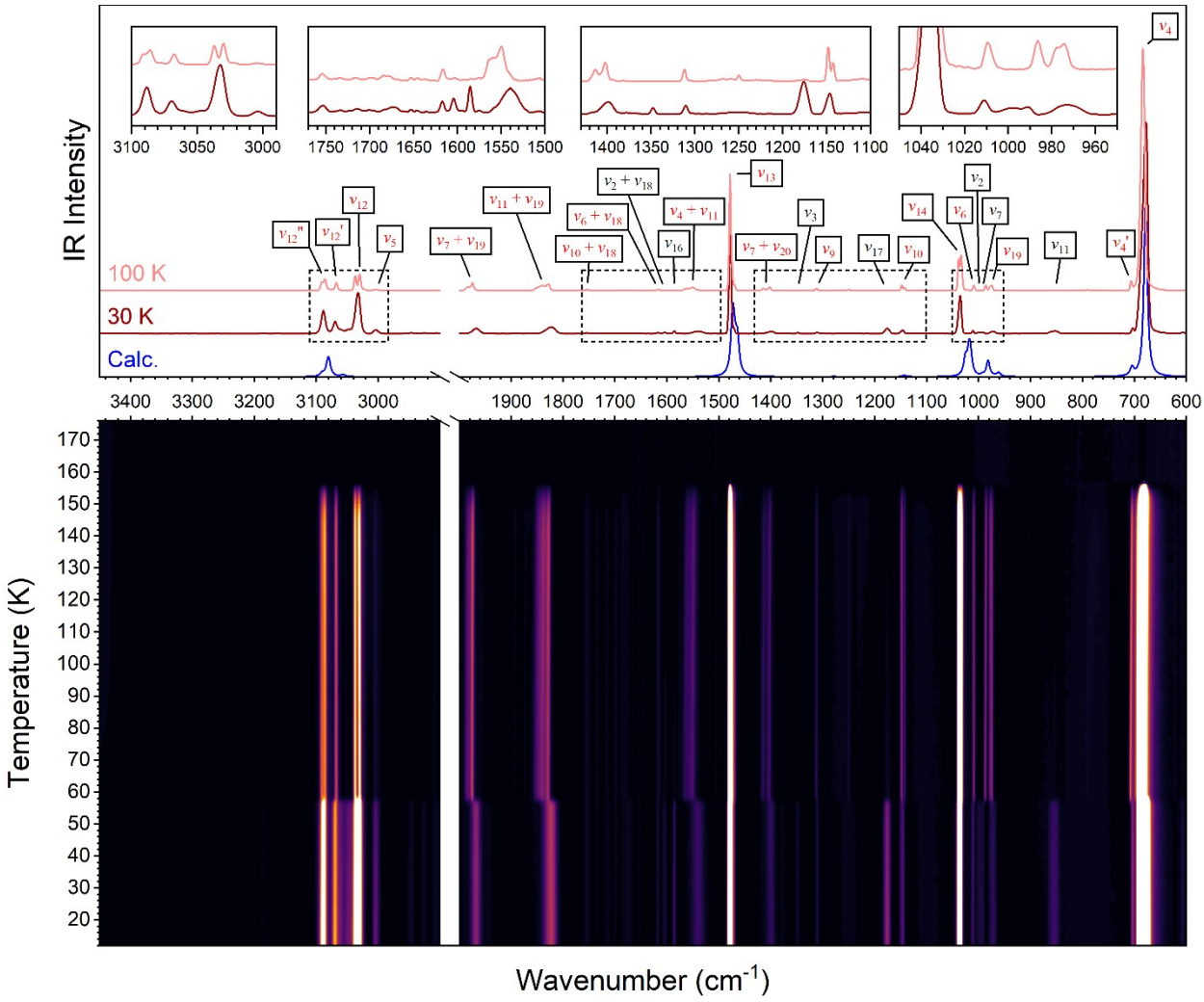

Figure S6. A heatmap of FTIR spectra of benzene ice recorded from 12-179 K at 2 cm^{-1} resolution (bottom), where lightness represents peak intensity. Contour spectra at 30, and 100 K (top) are shown in red. The theoretical spectrum calculated for the orthorhombic crystal polymorph (*Pbca* (61); Calc.) at the B3LYP-D3 level of theory is included for comparison in blue. Spectra are offset for clarity. Peak labels show assignments to benzene fundamental transitions and combination bands, where transitions belonging to symmetry species formally IR-active in the CPG of the Pbca space group (D_{2h}) are shown in red, and transitions only IR-active in the CPG of the $P\bar{1}$ space group (C_1) are shown in blue.

Table S6. IR peak assignments for C_6H_6 ice at 30 and 100 K. pDFT calculated frequencies are included for comparison and incorporate a 0.965 anharmonic scaling factor.

Peak (30 K) / cm-1	Peak (100 K) / cm-1	Peak (pDFT) / cm-1	Assignment	Reference †
3955 vw	3955 w		$\nu_3 + \nu_6 + (\nu_2 + \nu_{18})$	
3935 w	3930 w		$\nu_{11} + \nu_{12}$	a, b
3750 vw	3751 vw		unassigned	
3744 vw	3744 vw		unassigned	
3693, 3684 w	3697, 3690, 3681 w		unassigned	
3639 w	3642, 3635 w		$\nu_{12} + \nu_{18}$	a, b, d
3609 w	3609 w		$\nu_5 + \nu_{18}$	a, b, d
3186 vw	-		unassigned	
3164 vw	-		unassigned	
3088 s	3092, 3086 s	3075, 3068, 3063	ν_1, ν_{12}, ν_{15}, or $\nu_{13} + \nu_{16}$	a, b ,c
3069 s	3067 m		ν_1, ν_{12}, ν_{15}, or $\nu_{13} + \nu_{16}$	a, b ,c
3033 vs	3038, 3030 s	3046, 3045, 3039	ν_1, ν_{12}, ν_{15}, or $\nu_{13} + \nu_{16}$	a, b ,c
3004 m	3005 w	3020, 3018, 3015	ν_5	a, b ,c
2946 w 2926 w 2907 w	2908 vw		$\nu_9 + \nu_{16}$	a, b, d
2887 w	2888 w		unassigned	
2818 w	2818 w		$\nu_3 + \nu_{13}$	a, b, d
2650 w	2648 w		$\nu_{13} + \nu_{17}$	a, b, d
2613 w	2611 vw		$\nu_6 + \nu_{16} + \nu_{18}$	
2593 w	2593 w		$\nu_6 + \nu_{16}$	a, b, d
2382 w	2384, 2380 w		$\nu_3 + \nu_{14}$	a, b, d
2325 m	2325, 2321 w		$\nu_{10} + \nu_{17}$	a, b, d
2208 w	2209 w		unassigned	
2008 w	2013 w		unassigned	
1966 s	1983, 1975 s		$\nu_7 + \nu_{19}$	a, b, d
1822 s	1839, 1828 s		$\nu_{11} + \nu_{19}$	a, b, d
1755 w	1754 w		$\nu_{10} + \nu_{18}$	a, b, d
1618 w	1618 w		$\nu_6 + \nu_{18}$	a, b, d
1605 w	1603 vw		$\nu_2 + \nu_{18}$	a, b, d
1586 m	-		ν_{16}	a, b, c, d
1539 m	1565, 1550 s		$\nu_4 + \nu_{11}$	a, b, d
1477 vs 1472 vs	1478 vs 1469 vs	1478, 1477, 1477 1462, 1459, 1451	ν_{13}	a, b, c, d
1398 m	1415, 1403 m		$\nu_7 + \nu_{20}$	a, b, d
1348 w	-		ν_3	a, b, c, d
1310 w	1313 w	1293, 1291, 1291	ν_9	a, b, c, d

-	1250 w		unassigned	
1175 m	1175 w		ν_{17}	a, b, c, d
1146 m	1148, 1142 m	1136, 1134, 1130	ν_{10}	a, b, c, d
1035 vs	1039 s 1034 s	1045, 1029, 1028 1021, 1019, 1018	ν_{14}	a, b, c, d
1011 w	1009 m	1000, 1000, 999	ν_{6}	a, b, c, d
998 w	-		ν_{2}	a, c, d
991 w	-		ν_{7}	a, c, d
973 m	987 m 978, 974 m	996 989, 988, 985, 983, 980	ν_{19}	a, b, c, d
853 m	-		ν_{11}	a, b, c, d
703 m 676 vs	706 m 684 vs	710 693, 687	ν_{4}	a, b, c, d
607 m	-		$\nu 1_{8}$	a, c

Notes: † Peak assignments are compiled from liquid, amorphous and crystalline ice data published in (a, Nna-Mvondo & Anderson, 2022), (b, Mair & Hornig, 1949), (c, Shimanouchi, 1973), (d, Bertie & Keefe, 2004).

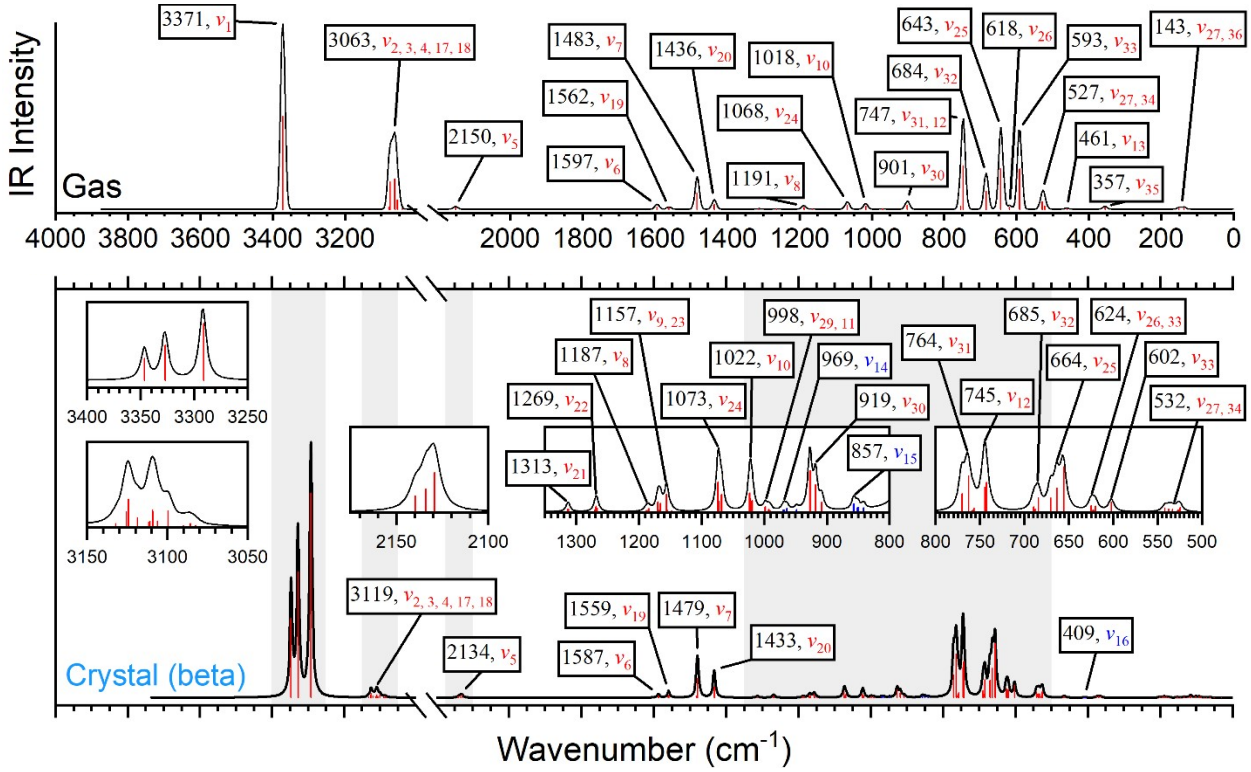

Figure S7. Theoretical IR spectra calculated using pDFT for the gas-phase (top) beta crystal-phase polymorph (bottom) of crystalline phenylacetylene at the B3LYP-D3, 6-311G(d) level of theory, with peaks labelled according to H-M notation and fit with a Gaussian line profile of 15 cm^{-1} width. The frequency of individual transitions formally IR-active and inactive in the gas-phase are shown in red and blue, respectively, with arbitrary absolute intensity. Spectra incorporate an anharmonic scaling factor of 0.965.

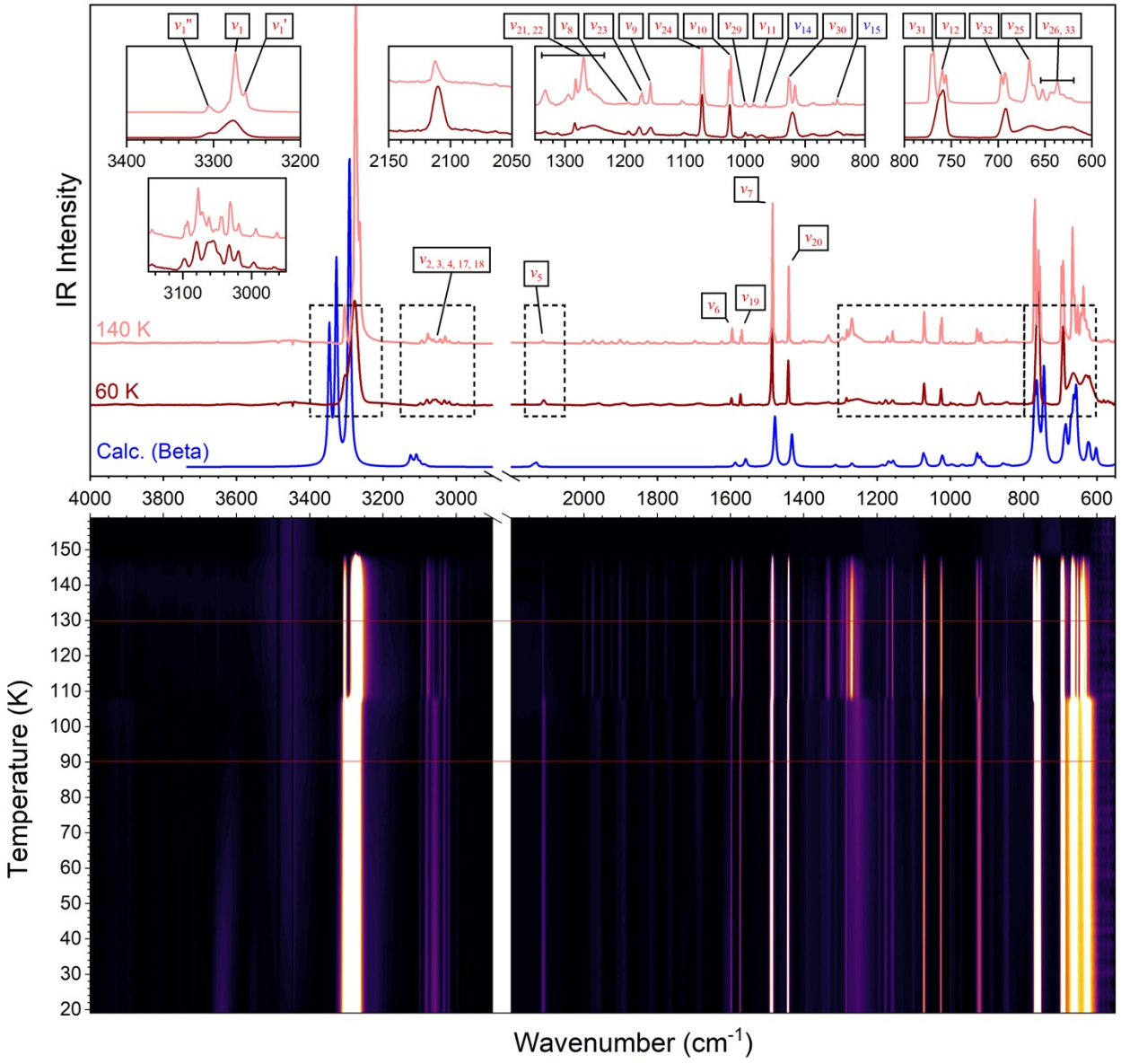

Figure S8. A heatmap of FTIR spectra of phenylacetylene ice recorded from 19-160 K at 2 cm^{-1} resolution (bottom), where lightness represents peak intensity. Contour spectra at 90, and 130 K (top) are shown in red. The theoretical spectrum calculated for the crystal beta-polymorph ($P\bar{1}$ (2)) at the B3LYP-D3 level of theory is included for comparison in blue. Spectra are offset for clarity. Peak labels show assignments to phenylacetylene fundamental transitions, where transitions belonging to symmetry species formally IR-active in MPG of phenylacetylene (C_{2v}) are shown in red, and transitions only IR-active in the CPG of the $P\bar{1}$; space group (C_1) are shown in blue.

Table S7. FTIR peak assignments for phenylacetylene thin-film ice at 90 and 130 K.

Peak (90 K) / cm^{-1}	**Peak (130 K) / cm^{-1}**	**Assignment**	**Reference †**
3929, 3889 vw	3925, 3913, 3894 vw	CB	
3652 vw	3651 vw	CB	
3614 vw	-	CB	
-	3368 vw	CB	
3340 w	3343 w	CB	
3304 m	3305 m	ν_1	a
3278 s	3282, 3275, 3264 vs	ν_1	a
3146 vw	3145 vw	CB	
3099 w	3096, 3093 w	ν_2, ν_3, ν_4, ν_{17}, ν_{18}	
3082 w	3077, 3072 w	ν_2, ν_3, ν_4, ν_{17}, ν_{18}	
3064, 3057 3048 w	3062, 3053 3045, 3043 w	ν_{17}, ν_3	a
3034 w	3031 w	ν_{18}	a
3021 w	3023, 3019 w	ν_4	a
2998 vw	2994 vw	CB	
2969 vw	2963 vw	CB	
2925 vw	2922 vw	CB	
2904 vw	-	CB	
2881 vw	2880 vw	CB	
2789 vw	2786 vw	CB	
2766 vw	2764 vw	CB	
2682 vw	2678 vw	CB	
2619 vw	2614 vw	CB	
2594 vw	2594, 2590 vw	CB	
2574 vw	2578 vw	CB	
2336 w	2333 w	CB	
2319 vw	2316 vw	CB	
2280 vw	2277 vw	CB	
2249 vw	2247 vw	CB	
2112 w	2113 w	ν_5	a, b
1975, 1959 w	2000 1976, 1965 1953, 1948 w	CB	
1903, 1892 w	1934, 1925 1902, 1897 1882 w	CB	b
1839, 1816 w	1852 1827 1813,1808 1800 w	CB	b
1708 w	1709 w	CB	
1682 w	1698, 1675 vw	CB	
1611 vw	1624 vw	CB	

1599 m	1596 m	ν_6	a
1590 w	1588 w	CB	
1574 m	1573, 1569 m	ν_{19}	a
1566 w	1563 vw	CB	
-	1550 vw	CB	
-	1536 vw	CB	
1487 s	1485, 1480 s	ν_7	a, b
1443 s	1442, 1434 s	ν_{20}	a
-	1401 vw	CB	
1389, 1384 w	1387, 1384 vw	CB	
1332 w	1333 m	ν_{21}, ν_{22}	a
-	1320 vw	ν_{21}, ν_{22}	
1312 w	1313 vw	ν_{21}, ν_{22}	
-	1295 m	ν_{21}, ν_{22}	
1285 m	1282 m	ν_{21}, ν_{22}	a
1273 w	1269 m	ν_{21}, ν_{22}	
1257 m	1258, 1249 w	ν_{21}, ν_{22}	
1195 w	1195	ν_8	a
1183 1176 w	1183 1174, 1172 w	ν_{23}	a
1157 w	1158 m	ν_9	a
1100 w	1106 w	CB	
1073 m	1072 m	ν_{24}	a, b
1026 1019 m	1027, 1024 1015 m	ν_{10}	a, b
1000 w	999, 997 vw	ν_{29}	a
991 w	987, 983 vw	ν_{11}	
972 w	966 vw	ν_{14}	a
921 m	928, 926 917 m	ν_{30}	a
888 w	887 w	CB	b
847 w	854, 847 w	ν_{15}	a
759 s	771, 769 759, 755 s	ν_{31} ν_{12}	a, b
691 s	697, 692 s	ν_{32}	
663 m	667, 662 652 s	ν_{25}	b
629, 621 m	644 636 632 624 s	ν_{26}, ν_{33}	b
532 m	532 s	ν_{27}, ν_{34}	a

Notes: † Peak assignments are compiled from liquid, amorphous and crystalline ice data published in (a, Chernia et al., 2001) and (b, Esposito et al., 2024). CB: Combination band.

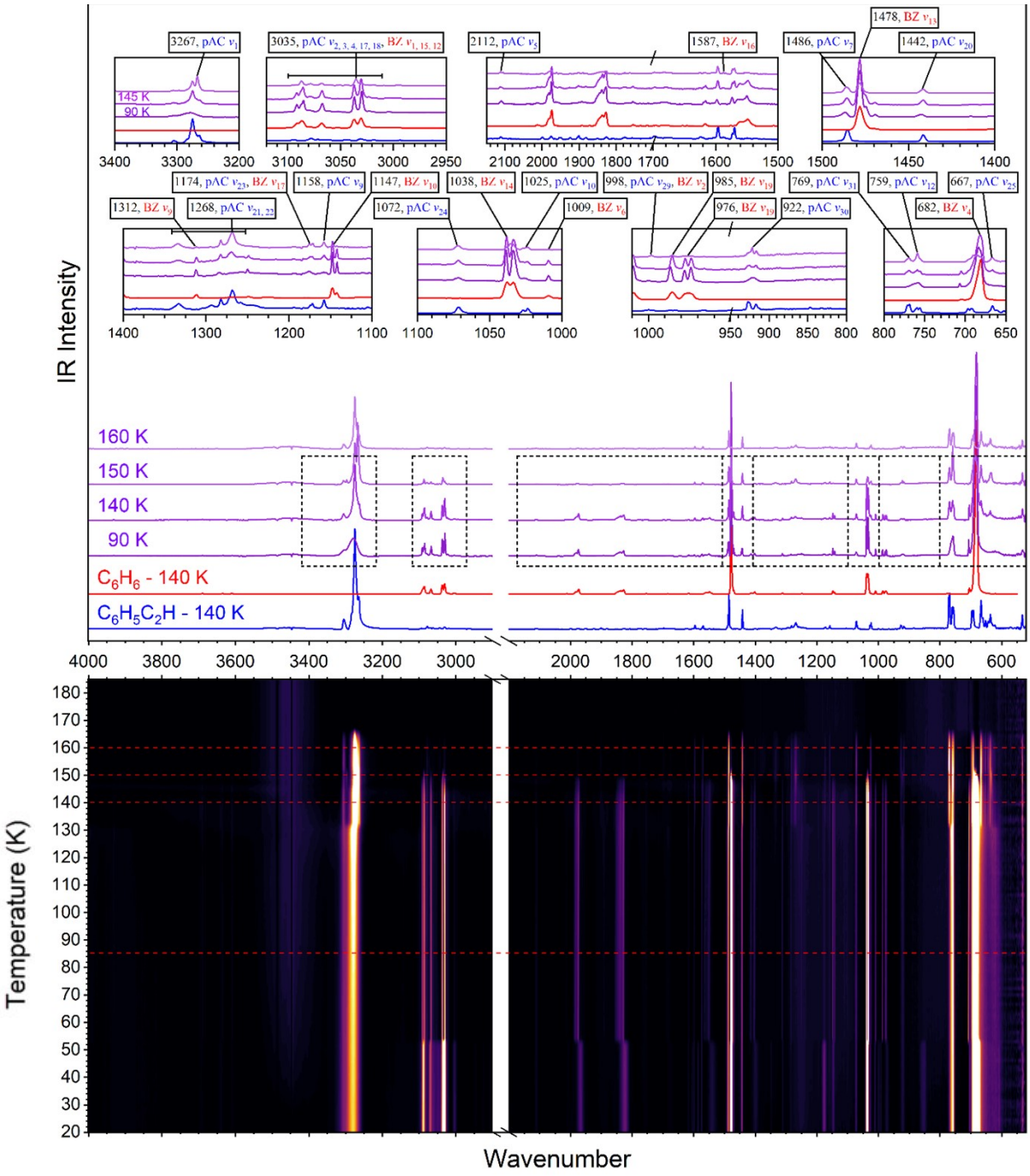

Figure S9. A heatmap of FTIR spectra of layered phenylacetylene/benzene ice recorded from 15-200 K at 2 cm^{-1} resolution (bottom), where lightness represents peak intensity. Contour spectra at 90, 140, 150, and 160 K (top) are shown in purple. For comparison, FTIR spectra of pristine benzene and phenylacetylene collected at 145 K are shown in red and blue, respectively. Peak labels (cm^{-1}) show assignments to benzene and phenylacetylene fundamental transitions in red and blue, respectively. Spectra are offset for clarity.

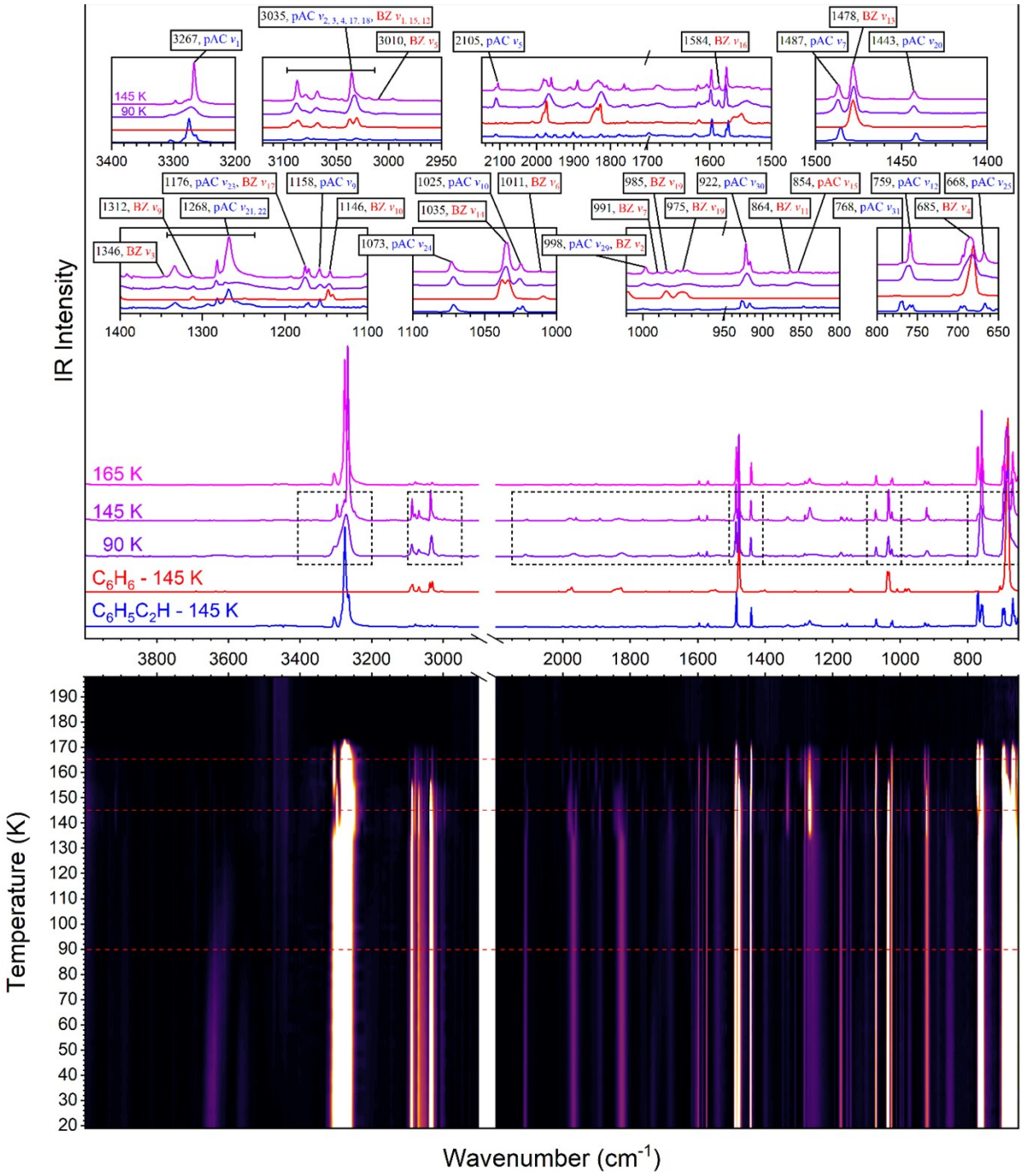

Figure S10. A heatmap of FTIR spectra of mixed phenylacetylene/benzene ice recorded from 15-200 K at 2 cm^{-1} resolution (bottom), where lightness represents peak intensity. Contour spectra at 90, 145, and 165 K (top) are shown in purple. For comparison, FTIR spectra of pristine benzene and phenylacetylene collected at 145 K are shown in red and blue, respectively. Peak labels (cm^{-1}) show assignments to benzene and phenylacetylene fundamental transitions in red and blue, respectively. Spectra are offset for clarity.

Table S8. FTIR peak assignments for co-deposited C_6H_6-$C_6H_5C_2H$ thin-film ice measured at 65, 95, and 150 K to C_6H_6 and $C_6H_5C_2H$ fundamentals.

Peak (90 K) / cm^{-1}	**Peak (145 K) / cm^{-1}**	**Peak (165 K) / cm^{-1}**	**Assignment**
3305, 3271	3296, 3282, 3276, 3267	3305, 3285, 3275, 3264	$C_6H_5C_2H$ ν_1
3105-3000	3105-3000	3105-3000	$C_6H_5C_2H$ $\nu_{2,\ 3,\ 4,\ 17,\ 18}$ C_6H_6 $\nu_{1,\ 15,\ 12,\ 5}$
2110	2105	2112	$C_6H_5C_2H$ ν_5
1597	1596	1596	$C_6H_5C_2H$ ν_6
1585	1584	-	C_6H_6 ν_{16}
1573	1573	1573, 1570	$C_6H_5C_2H$ ν_{19}
1487	1491, 1487	1485	$C_6H_5C_2H$ ν_7
1478, 1471	1478, 1470	-	C_6H_6 ν_{13}
1443	1443	1441	$C_6H_5C_2H$ ν_{20}
1346	1346	-	C_6H_6 ν_3
-	1334	1333	$C_6H_5C_2H$ $\nu_{21,\ 22}$
1311	1312	-	C_6H_6 ν_9
1284	1282 1268	1282 1269	$C_6H_5C_2H$ $\nu_{21,\ 22}$
1194	1193	1194	$C_6H_5C_2H$ ν_8
1176	1176, 1171	1172	$C_6H_5C_2H$ ν_{23} C_6H_6 ν_{17}
1158	1158	1158	$C_6H_5C_2H$ ν_9
1146	1145	-	C_6H_6 ν_{10}
1072	1073	1072	$C_6H_5C_2H$ ν_{24}
1035	1035	-	C_6H_6 ν_{14}
1026	1025	1027, 1023	$C_6H_5C_2H$ ν_{10}
1011	1012	-	C_6H_6 ν_6
999	998	998	$C_6H_5C_2H$ ν_{29} C_6H_6 ν_2
991	991	-	C_6H_6 ν_7
973	986, 979, 974	-	C_6H_6 ν_{19}
921	922, 916	923, 925, 917	$C_6H_5C_2H$ ν_{30}
857	864	-	C_6H_6 ν_{11}
857	854	847	$C_6H_5C_2H$ ν_{15}
761	768	771, 770	$C_6H_5C_2H$ ν_{31}
761	759	759, 756	$C_6H_5C_2H$ ν_{12}
704 783	704 694, 685	 697, 692	C_6H_6 ν_4 $C_6H_5C_2H$ ν_{32}
666	668	667, 661 653	$C_6H_5C_2H$ ν_{25}

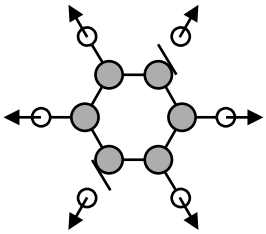	ν_1	A_{1g}	CH S. Str	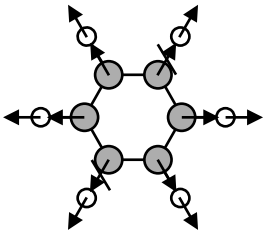	ν_2	A_{1g}	Breathing	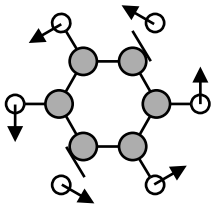	ν_3	A_{2g}	Propeller	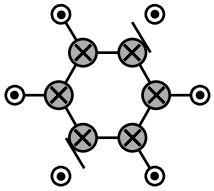	ν_4	A_{2u}	CH S. Wag
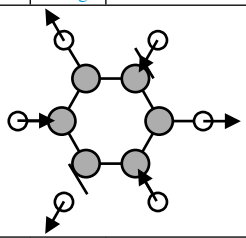	ν_5	B_{1u}	3F CH Str	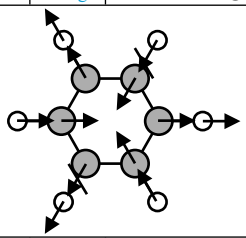	ν_6	B_{1u}	3F CC Bre	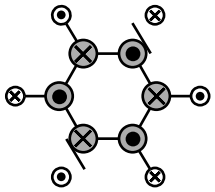	ν_7	B_{2g}	3F CH Wag	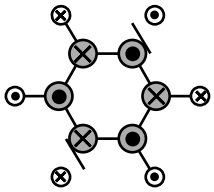	ν_8	B_{2g}	3F CC Wag
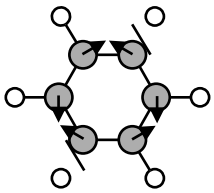	ν_9	B_{2u}	3F CC Ben	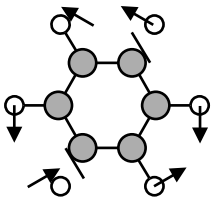	ν_{10}	B_{2u}	3F CH Ben								
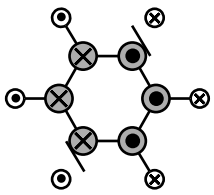	ν_{11}	E_{1g}	2F CH Wag	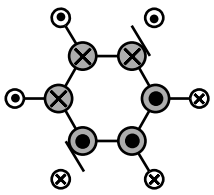	ν_{12}	E_{1u}	2F CH Str	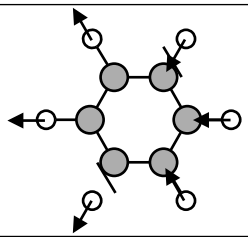				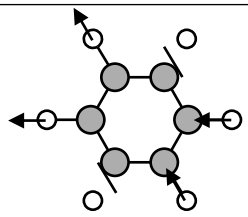			
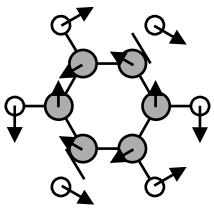	ν_{13}	E_{1u}	AS. Swim	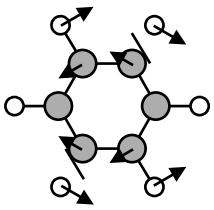	ν_{14}	E_{1u}	S. Swim	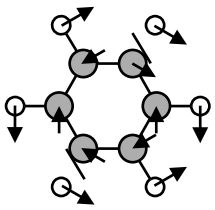				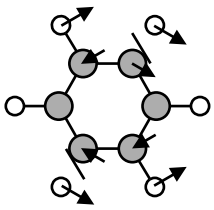			
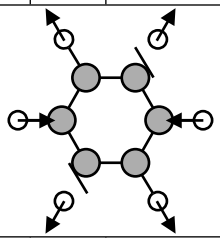	ν_{15}	E_{2g}	CH Pinch	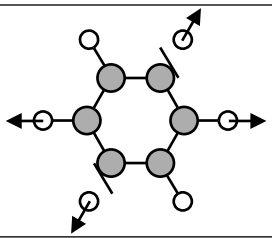	ν_{16}	E_{2g}	Ring Elongation	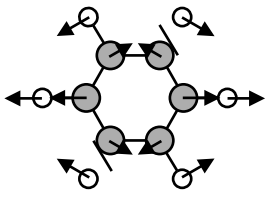				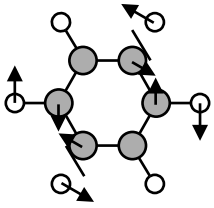			

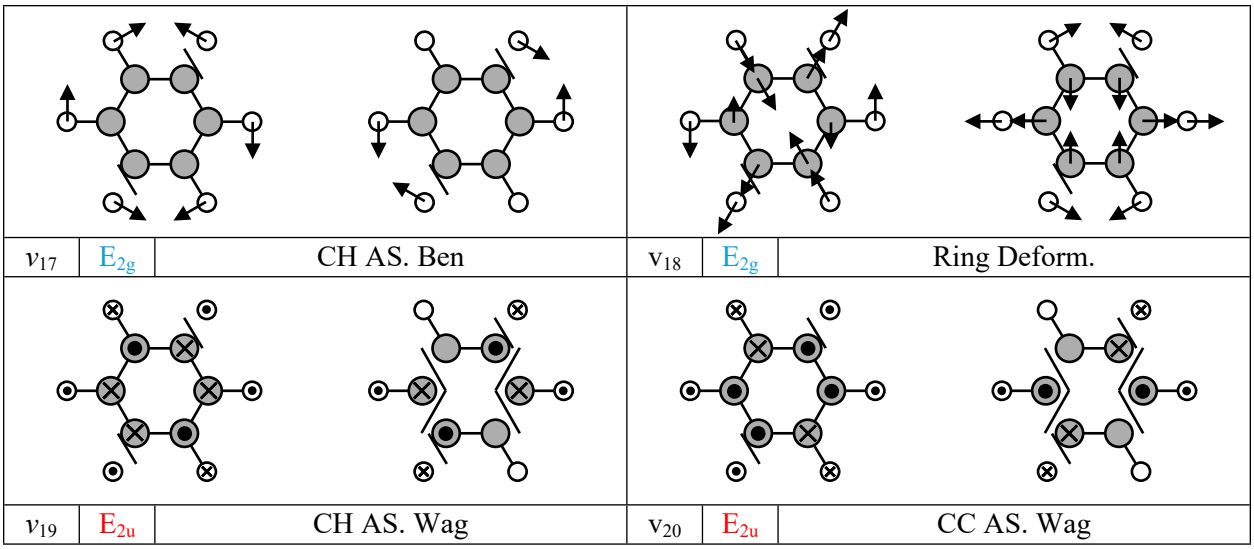

Figure S11. Atomic displacement vectors, molecular symmetry species, and description label for the vibrational modes of the C_6H_6 molecule generated by visualization of DFT calculations. Modes are numbered according to H-M notation. Infrared-active symmetry species of the molecular point-group (D_{6h}) are indicated in red, and Raman-active species are depicted in blue. Abbreviations: S- symmetric, AS- asymmetric, Str- stretch, Ben- in-plane bend, Wag- out-of-plane bend, 2F- two-fold rotationally symmetric, 3F- three-fold rotationally symmetric. Not to scale

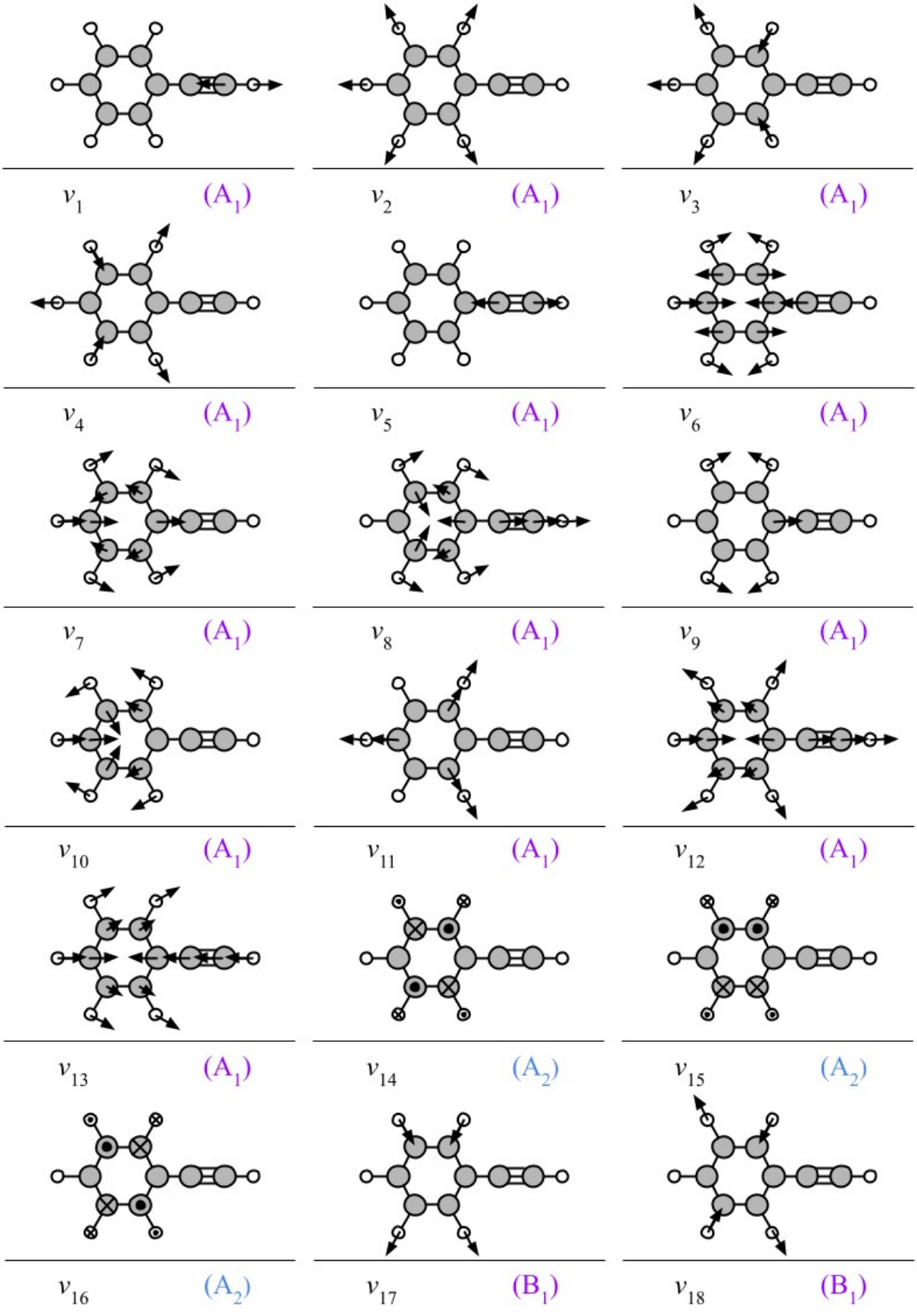
ν_1 (A_1)
ν_2 (A_1)
ν_3 (A_1)
ν_4 (A_1)
ν_5 (A_1)
ν_6 (A_1)
ν_7 (A_1)
ν_8 (A_1)
ν_9 (A_1)
ν_{10} (A_1)
ν_{11} (A_1)
ν_{12} (A_1)
ν_{13} (A_1)
ν_{14} (A_2)
ν_{15} (A_2)
ν_{16} (A_2)
ν_{17} (B_1)
ν_{18} (B_1)

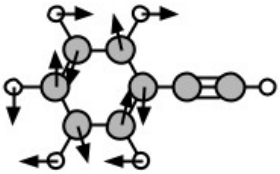

ν_{19} (B_1)

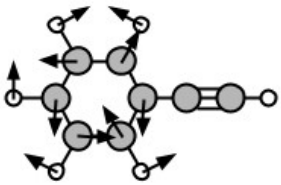

ν_{20} (B_1)

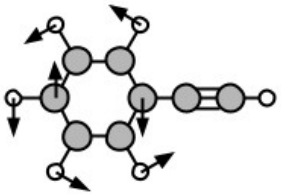

ν_{21} (B_1)

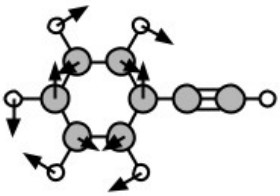

ν_{22} (B_1)

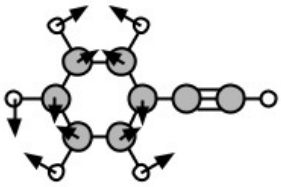

ν_{23} (B_1)

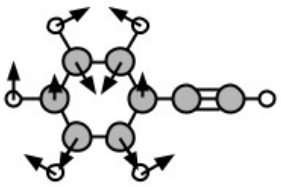

ν_{24} (B_1)

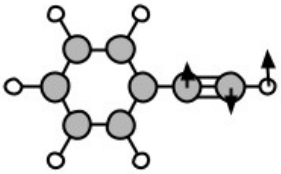

ν_{25} (B_1)

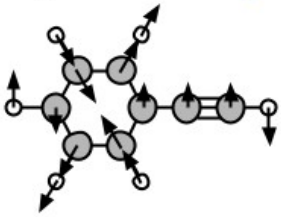

ν_{26} (B_1)

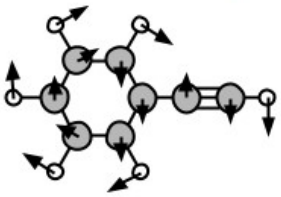

ν_{27} (B_1)

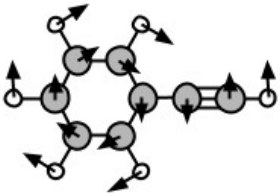

ν_{28} (B_1)

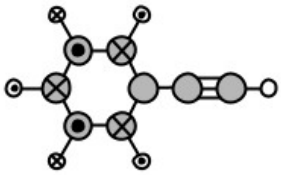

ν_{29} (B_2)

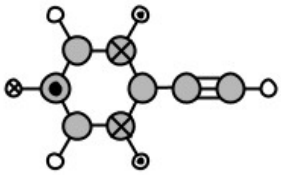

ν_{30} (B_2)

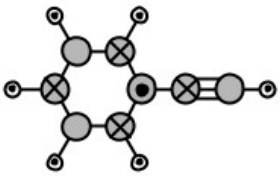

ν_{31} (B_2)

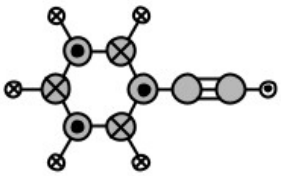

ν_{32} (B_2)

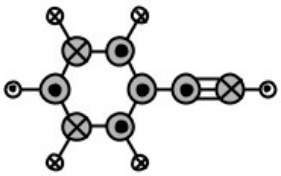

ν_{33} (B_2)

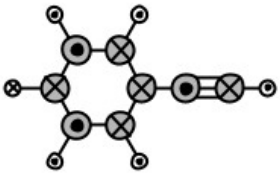

ν_{34} (B_2)

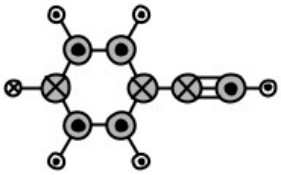

ν_{35} (B_2)

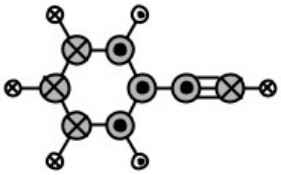

ν_{36} (B_2)

Figure S12. Atomic displacement vectors and molecular symmetry species for the vibrational modes of the $C_6H_5C_2H$ molecule generated by visualization of DFT calculations. Modes are numbered according to H-M notation. Raman-active symmetry species of the molecular point-group (D_{2h}) are indicated in blue, and species both IR and Raman-active are depicted in purple. Not to scale.

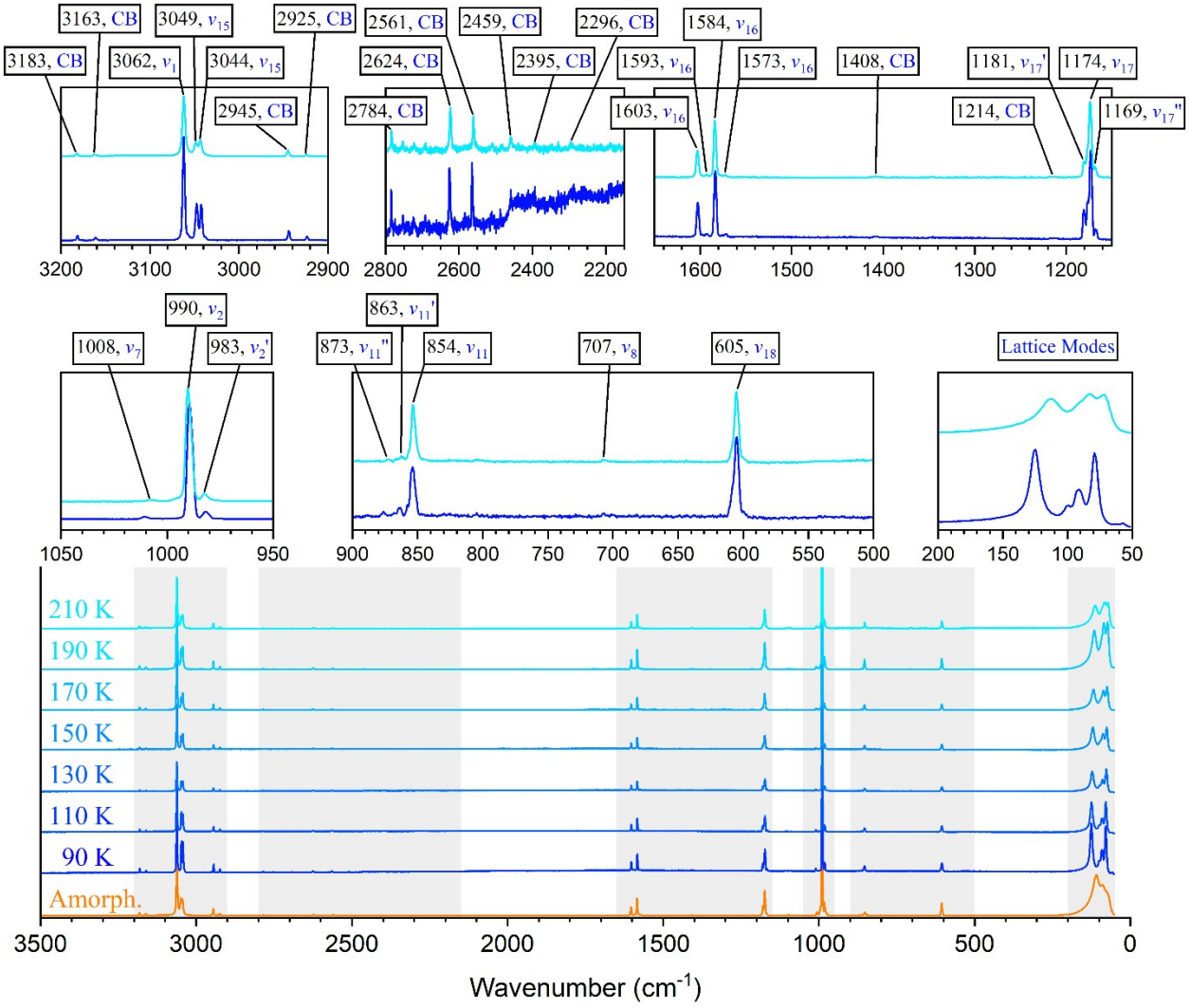

Figure S13. Raman spectra of pristine C_6H_6 ice collected between 90 and 210 K, and an amorphous ice spectrum collected after direct liquid deposition at 223 K. Features are assigned by comparison to pDFT calculations and literature. Combination bands are denoted "CB". 90 and 210 K spectra shown in inset.

Table S9. Raman peak assignments for C_6H_6 ice at 90 and 210 K. pDFT calculated frequencies are included for comparison and incorporate a 0.965 anharmonic scaling factor.

Peak (90 K) / cm^{-1}	**Peak (210 K) / cm^{-1}**	**Calculated Peak / cm^{-1}**	**Assignment**	**Reference †**
3181	3182		CB	
3162	3162		CB	
3062	3062	3099, 3092	ν_1	a
3048, 3042	3048, 3043	3080, 3079, 3078	ν_5	a
2944	2945		CB	
2924	2924		CB	
2785	2783		CB	
2752	2755		CB	
2725	2721		CB	
2693	2693		CB	
2626	2625		CB	
2565	2561		CB	
2510	2509		CB	
2487	2485		CB	
2459	2458		CB	
2394	2394		CB	
2330	2328		CB	
2288	2295		CB	
2187	2187		CB	
1603, 1593 1583, 1573	1603, 1593 1584, 1572	1579, 1578 1576, 1574	ν_{16}	a
1407	1408		CB	
1347	1345		CB	
1213	1215		CB	
1180 1176, 1173 1168	1180 1174 1168	1169, 1167 1166, 1164 1160, 1153	ν_{17}	a
1010	1008	1011, 1007	ν_7	a
990 982	990 983	991 982, 981 979	ν_2	a
876 864 854	873 862 853	875, 873 865 859, 852 849, 848, 842	ν_{11}	a
805	804		CB	
708	707	705, 704 699	ν_8	a
605	605	609, 608 606, 604 603, 602	ν_{18}	a

125	113	Lattice Modes
100	83	
92	72	
79		
57		

Notes: † Peak assignments are compiled from liquid, amorphous and crystalline ice data published in (a, Shimanouchi, 1973).

Table S10. Unit cell parameters and phase fraction for the Rietveld refinement of the literature H_2O and C_6H_6 unit cells, and the C_6H_6 + $C_6H_5C_2H$ $P2_1$ co-crystal unit cell solution against XRD diffraction pattern collected at 200 K.

Lattice parameters	**H_2O (I_h)**	**C_6H_6 (ortho.)**	**C_6H_6 + $C_6H_5C_2H$ *$P2_1$* co-crystal**
200 K pattern: Rw = 19.27%, GOF = 20.68			
a	4.51142 Å	7.48988 Å	11.89385 Å
b	4.51142 Å	9.45708 Å	8.33415 Å
c	7.3498 Å	6.96334 Å	5.60863 Å
α	90°	90°	90°
β	90°	90°	96.866°
γ	120°	90°	90°
Volume	129.549 Å^3	493.230 Å^3	551.969 Å^3
Molar fraction	N/A	0.816	0.81

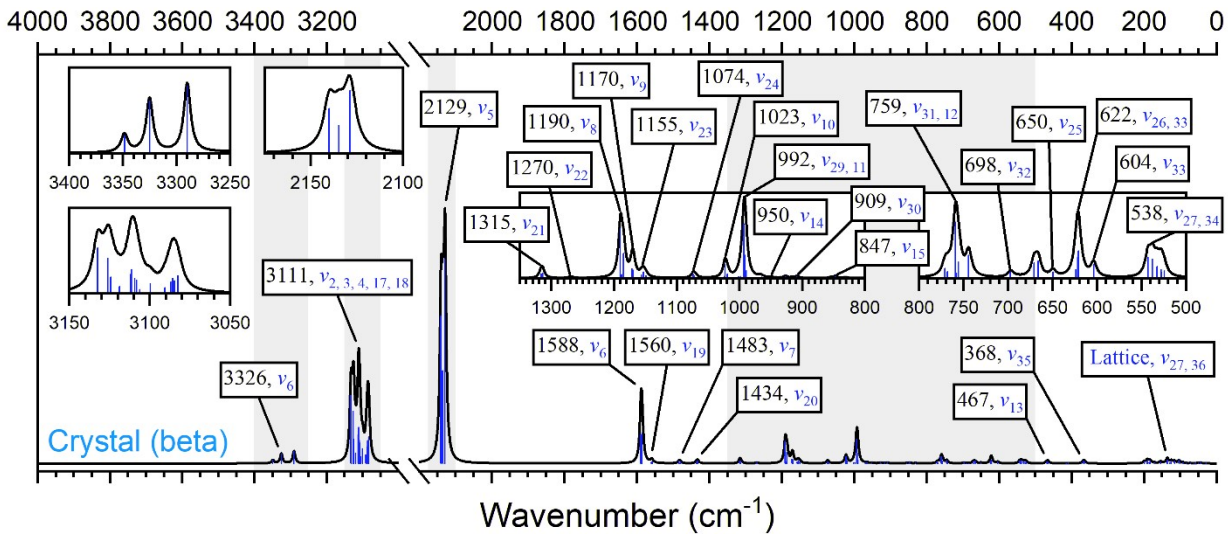

Figure S14. Theoretical Raman spectra calculated using pDFT for the beta polymorph of crystalline phenylacetylene at the B3LYP-D3, 6-311G(d) level of theory, with peaks labelled according to H-M notation and fit with a Gaussian line profile of 15 cm^{-1} width. The frequency of individual transitions formally IR-active in the gas-phase are shown in blue. Spectra incorporate an anharmonic scaling factor of 0.965.